PNAS RESEARCH ARTICLE | BIOCHEMISTRY

Phagocytes as plaque catalysts: Human macrophages generate seeding-competent Aβ42 fibrils with cross-seeding activity

Katerina Konstantoulea[a,b], Meine Ramakers[a,b], Sarah C. Borrie[a,c], Dries T'Syen[a,c], Daan Moechars[a,c], Malgorzata A. Sliwinska[a,c,d], Brajabandhu Pradhan[a,b], Giulia Albertini[a,c], Nóra Baligács[a,c], Grigoria Tsaka[a,b], Bert Houben[a,b], Mark Fiers[a,c], Rodrigo Gallardo[a,b], Maarten Dewilde[e,f], Dietmar Rudolf Thal[g,h], Michael Willem[i], Jonas J. Neher[i,j,k], Bart De Strooper[a,c], Frederic Rousseau[a,b,1], and Joost Schymkowitz[a,b,1]

Affiliations are included on p. 11.

Edited by Judith Frydman, Stanford University, Stanford, CA; received June 26, 2025; accepted January 21, 2026

The prevailing view frames microglia and macrophages as guardians against amyloid beta (Aβ) accumulation in Alzheimer's disease (AD). Here, we overturn this paradigm by demonstrating that human phagocytic cells, including differentiated THP-1 macrophages and hESC-derived microglia, are not merely passive responders but active producers of extracellular, seeding-competent Aβ42 fibrils, the amyloid species most strongly linked to parenchymal plaque formation and neurodegeneration. These cell-generated aggregates differ structurally and functionally from synthetic fibrils, displaying enhanced seeding and tau cross-seeding activity in biosensor models. Notably, Aβ42 fibril formation in this system requires active cellular processes and is exacerbated by loss of Triggering Receptor Expressed on Myeloid Cells 2 (TREM2), a major AD risk gene. Transcriptomic profiling reveals an early inflammatory response resembling microglial states observed in human AD models. Together, these findings support emerging evidence from in vivo studies that macrophages and microglia can influence amyloid seeding and introduce a human-relevant in vitro platform to explore how Aβ aggregation intersects with innate immune function and genetic risk. Our results reinforce the concept that microglia may play a dual role in AD, acting both as responders and inadvertent facilitators of amyloid assembly, with implications for early therapeutic intervention.

Alzheimer's disease | microglia | TREM2 | Ab42

Significance

How amyloid plaques emerge and spread in Alzheimer's disease remains a critical unanswered question. Here, we show that human immune cells, including brain-resident microglia, can actively generate Aβ42 fibrils, the form of amyloid most strongly linked to neurodegeneration. These cell-produced fibrils not only seed further amyloid buildup but also trigger tau aggregation, a key event in disease progression. We further demonstrate that genetic risk factors like TREM2 (Triggering Receptor Expressed on Myeloid Cells 2) amplify this process. Our findings reveal a direct link between immune cell activity, genetic susceptibility, and the earliest stages of Alzheimer's pathology, offering insights into disease mechanisms and potential intervention points.

Alzheimer's disease (AD) is a progressive neurodegenerative disorder that remains a major global health challenge due to its increasing prevalence (1, 2). Central to AD pathology is the accumulation of amyloid beta (Aβ) plaques, particularly fibrils composed of Aβ42, a highly aggregation-prone peptide (3). The enhanced aggregation and seeding potential of Aβ42 compared to Aβ40 underlie its strong association with disease progression (4, 5), including its role in initiating tau pathology and driving neuroinflammation (6). Current amyloid therapies targeting Aβ aggregates represent a significant advancement in the treatment of AD. To date, three monoclonal antibodies have received U.S. Food and Drug Administration approval for this purpose. Aducanumab, derived from memory B cells of cognitively normal elderly individuals, binds parenchymal Aβ and has been shown to reduce both amyloid plaque burden and cognitive decline (7, 8). Lecanemab, developed from the mouse antibody mAb158, targets soluble Aβ aggregates and has demonstrated efficacy in slowing clinical progression and clearing Aβ deposits (7, 9, 10). Donanemab, based on the mouse antibody mE8-IgG2a, targets explicitly the pyroglutamate-modified N terminus of Aβ, a form enriched in amyloid plaques, and has shown benefits in individuals with early symptomatic AD or mild cognitive impairment (11–13). Despite extensive research in Aβ pathology and therapeutic development, critical gaps remain in understanding the cellular mechanisms that regulate Aβ aggregation and their contribution to AD progression.

Microglia, the brain's resident immune cells, are increasingly recognized as central players in the formation and propagation of Aβ plaques. They exhibit a dual role: On the one hand, microglia clear Aβ aggregates through phagocytosis (14, 15); on the other they can promote aggregation and contribute to amyloid seeding (16–18). For example, depletion of the microglial niche in a mouse of Aβ pathology led to a reduction in plaque load (19). The opposing functions of microglia are implicated in the early stages of AD, where immune dysregulation may shift microglial activity toward amyloid propagation and inflammation (20). Understanding how microglia interact with Aβ42 and their role in plaque formation is crucial for unraveling the complex interplay between amyloid deposition and neuroinflammation.

Author contributions: K.K., M.R., J.J.N., B.D.S., F.R., and J.S. designed research; K.K., M.R., S.C.B., D.T., D.M., M.A.S., B.P., G.A., G.T., and R.G. performed research; N.B., M.D., D.R.T., M.W., and J.J.N. contributed new reagents/analytic tools; K.K., M.R., D.T., D.M., M.A.S., B.P., G.A., G.T., B.H., M.F., B.D.S., F.R., and J.S. analyzed data; and K.K., B.D.S., F.R., and J.S. wrote the paper.

The authors declare no competing interest.

This article is a PNAS Direct Submission.

[1]To whom correspondence may be addressed. Email: Frederic.rousseau@kuleuven.be or joost.schymkowitz@kuleuven.be.

This article contains supporting information online at https://www.pnas.org/lookup/suppl/doi:10.1073/pnas.2516774123/-/DCSupplemental.

Published March 2, 2026.

In vitro models that capture microglial behavior are essential tools for mechanistic studies of amyloid aggregation and innate immune responses. THP-1 macrophages, a human monocytic cell line, have previously been shown to support amyloid formation, particularly with Aβ40, a peptide more commonly associated with cerebral amyloid angiopathy and vascular pathology (21, 22). In contrast, Aβ42 is more directly implicated in parenchymal plaque formation and neurodegeneration (4, 5), making it a more relevant target for modeling AD pathophysiology. Studying Aβ42 aggregation in vitro therefore presents a more disease-relevant but also more challenging scenario. Moreover, although macrophages and microglia share phagocytic functions, they exist in distinct anatomical and immunological niches (23). As such, it cannot be assumed that macrophage cell lines will faithfully replicate microglial behavior, particularly in the context of Aβ42 aggregation and associated inflammatory responses.

TREM2 (Triggering Receptor Expressed on Myeloid Cells 2) has emerged as a critical regulator of microglial function in AD. Genetic variants in TREM2, such as the R47H substitution, are among the strongest risk factors for late-onset sporadic AD after apolipoprotein (24–26). These variants are associated with increased amyloid burden and tau pathology, and loss of TREM2 function impairs microglial ability to respond to plaques (25, 27). Functionally, TREM2 mediates microglial lipid sensing, cell survival, and transition to disease-associated states that promote plaque compaction and modulate neurodegeneration (28). These insights emphasize the need for in vitro models capable of capturing TREM2-regulated microglial dynamics, a gap this study seeks to fill.

In light of these challenges, a key goal is to establish in vitro models that not only replicate microglial responses to Aβ42 but also respond to AD-relevant genetic perturbations. Here, we show that THP-1 macrophages not only promote the extracellular deposition of Aβ42 fibrils with distinct structural and functional properties but also recapitulate key features of early microglial responses, including cytokine-driven inflammation (29) and sensitivity to TREM2 perturbation (30). Using transcriptomic comparisons with human embryonic stem cell(hESC)-derived microglia and genetic perturbations in both THP-1 and EPSC-derived microglia, we demonstrate that THP-1 cells represent a tractable and biologically relevant system for studying amyloid-associated innate immune processes. Our findings provide a framework for understanding the role of macrophages in amyloid aggregation and inflammation and establish a relevant model for studying early-stage mechanisms in AD and for evaluating therapeutic interventions.

Results

THP-1 Macrophages Induce Extracellular Amyloid Deposition of Aβ42. To investigate the potential for THP-1 macrophages to deposit Aβ42 aggregates, we differentiated THP-1 cells into macrophages using 50 ng/mL PMA for 48 h. The differentiated macrophages were then incubated with freshly dissolved Aβ42 at various concentrations for an additional 48 h (Fig. 1*A*). Initially, we tested deposition in the presence and absence of 100 μg/mL (~22 μM) Aβ42. Staining with Congo red, the gold-standard dye used for diagnosing amyloidosis due to its apple-green birefringence under polarized light (31), revealed the expected birefringence in the presence of 100 μg/mL Aβ42, indicating amyloid formation and deposition (Fig. 1*B*). No birefringence was observed in control samples lacking Aβ42 (Fig. 1*B*).

To further confirm amyloid deposition, we stained the samples with pFTAA (32) and Amytracker680, two fluorescent dyes specific to amyloid-rich structures. Both dyes exhibited strong fluorescence signals in the presence of Aβ42, confirming the presence of amyloid aggregates (Fig. 1 *C* and *D*). Importantly, no deposition was observed in the absence of cells, indicating that they are necessary for Aβ42 deposition (*SI Appendix*, Fig. S1*A*).

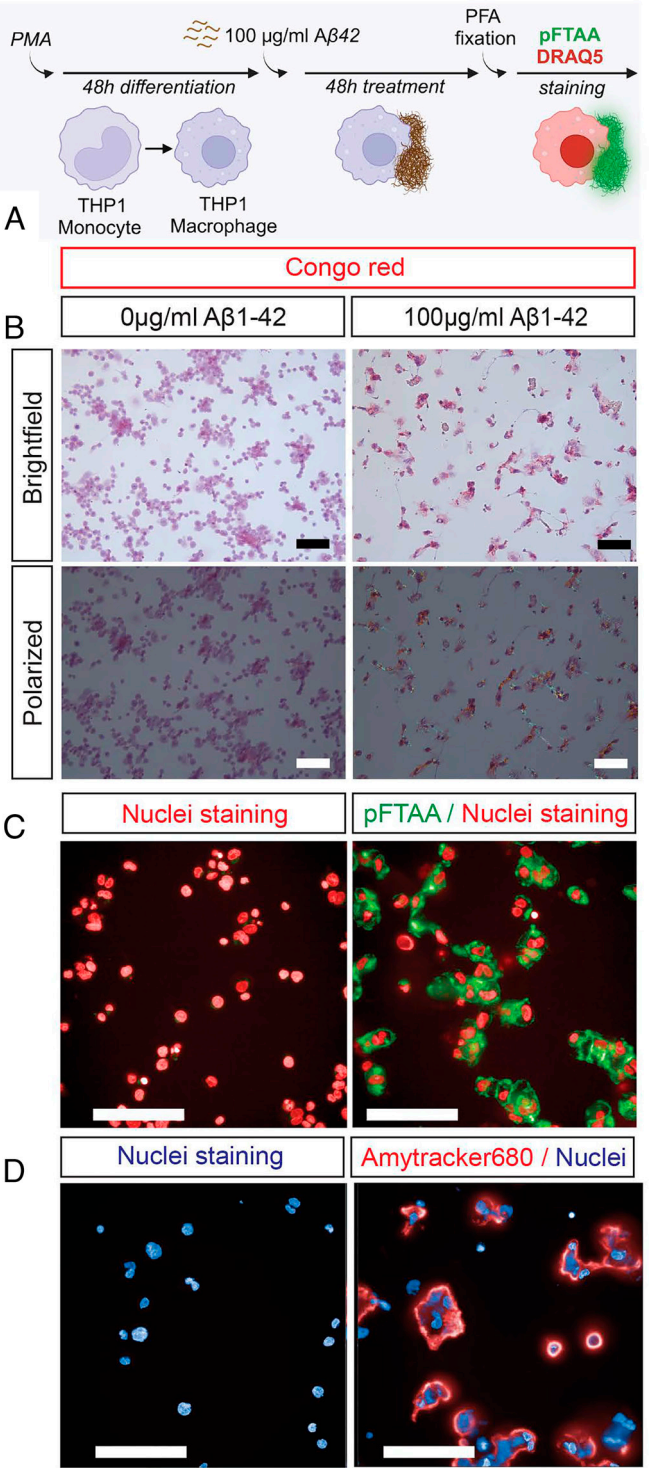

Fig. 1. THP-1 cells deposit amyloid fibrils. (*A*) Schematic of experimental procedure. (*B*) Congo Red staining in the absence or presence of rAβ42 (0, 100 μg/mL). The panels above are the cells under Brightfield. The panels below are the cells under polarized light. Light green-blue and yellow color indicates amyloid formation. Purple color: hematoxylin. Red: Congo red. (Scale bar, 50 μM.) (*C*) pFTAA staining in the presence and absence of rAβ42 (0, 100 μg/mL). Green: pFTAA, red: nuclei staining. (Scale bar, 100 μm.) (*D*) Amytracker680 staining in the presence and absence of rAβ42 (0, 100 μg/mL). Red: amytracker, blue: nuclei staining. (Scale bar, 100 μm.)

Next, we examined Aβ42 deposition across a range of concentrations (0 to 100 μg/mL). Differentiated macrophages were treated with increasing concentrations of Aβ42, followed by pFTAA staining. Quantification of fluorescence intensity revealed a dose-dependent increase in Aβ42 deposition, with significant accumulation detected at concentrations above 30 μg/mL (Fig. 2 *A* and *B*). Quantifying the surface area stained by pFTAA gave similar results (*SI Appendix*, Fig. S1*C*).

To determine whether the aggregates formed in this model were primarily accumulating in the extracellular space, we employed the Trypan blue quenching technique. This method utilizes Trypan blue's ability to absorb green fluorescence and its exclusion from

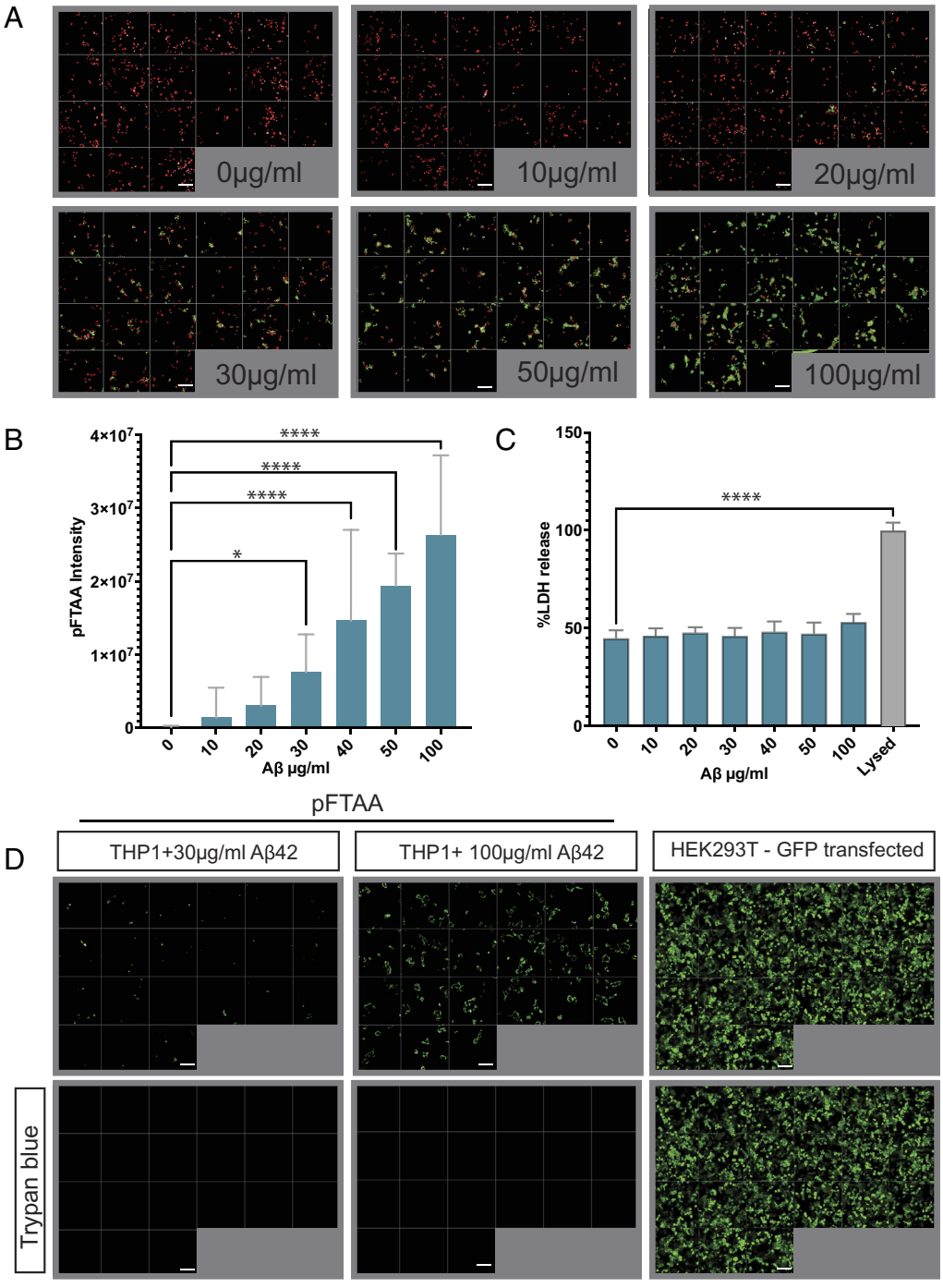

Fig. 2. THP-1 cells have significant rAβ42 extracellular deposition. (*A*) Images of Aβ deposition in seven different rAβ42 concentrations. 21 different fields are shown for each concentration. Red: nuclei (DAPI), Green: aggregates (pFTAA). (Scale bar, 100 μm.) (*B*) Bar plot of pFTAA intensity of THP-1 cells with increasing concentration of rAβ. Four independent experiments with four repeats, mean + SD. Statistics: Ordinary one-way ANOVA with Dunnett correction for multiple comparisons. *<0.05, ****<0.0001. (*C*) %LDH release in the presence of increasing concentrations of rAβ42. 100% indicates release of lysed cells. Two independent experiments with two repeats, mean + SD. Statistics: Ordinary one-way ANOVA with Dunnett correction for multiple comparisons. ****<0.0001. (*D*) Live imaging of THP-1 cells incubated with 30 μg/mL or 100 μg/mL rAβ42 and stained with pFTAA (*Upper* panels, *Left* and *Middle*). *Lower* panels show the same wells after addition of Trypan Blue (*Lower* panel, *Left* and *Middle*). The *Right Upper* panel shows live imaging of HEK293T cells transfected with green fluorescent protein (GFP). The *Right Lower* panel shows the same well after addition of Trypan Blue, indicating that Trypan blue successfully quenches extracellular pFTAA staining. (Scale bar, 100 μm.)

live cells. Live cells stained with pFTAA were imaged before and after Trypan blue addition. At both 30 μg/mL and 100 μg/mL Aβ42, most fluorescence was quenched, confirming that the majority of aggregates were extracellular at the time of detection (Fig. 2*D*, *Left* and *Middle*). As a control, GFP-expressing HEK cells were similarly treated, and GFP fluorescence persisted after Trypan blue addition, confirming intracellular localization of GFP (Fig. 2*D*, *Right*).

Finally, we assessed cell viability using an lactate dehydrogenase (LDH) release assay, which detects membrane disruption. No significant reduction in cell viability was observed, even at 100 μg/mL Aβ42, though a slight but nonsignificant increase in LDH release was noted at this concentration (Fig. 2*C*). This finding was supported by nuclear counts, which showed no differences in cell numbers after Aβ42 treatment (*SI Appendix*, Fig. S1*B*). Interestingly, treated macrophages displayed morphological changes, likely reflecting their activation and capacity to respond to Aβ42, consistent with macrophage plasticity in different activation states.

Aggregation-Prone Aβ42 and Active Macrophages Are Essential for Amyloid Deposition. To verify that the observed deposition of THP-1 cells results from Aβ42 aggregation, we incubated differentiated THP-1 cells with a nonaggregating Aβ42 variant (Scrambled-Aβ42). Scrambled-Aβ42 contains the same amino acids as Aβ42 but has no aggregation propensity as predicted by the TANGO algorithm (33) (*SI Appendix*, Fig. S2*A*). Additionally, Thioflavin T, a dye frequently used to monitor aggregation (34), did not detect amyloid formation of Scrambled-Aβ42 in the concentrations used (10, 20, 30, 40, 50, 100 μg/mL) (*SI Appendix*, Fig. S2 *B–D*). Accordingly, we detected no amyloid deposition upon incubation of THP-1 macrophages with different concentrations of Scrambled-Aβ42 (Fig. 3 *A* and *D*).

To ensure that the observed deposition requires cellular activity and is not simply the result of Aβ42 nucleation by cell membranes or other cellular components, we fixed the differentiated THP-1 cells with 4% paraformaldehyde (PFA) before incubation with Aβ42. We chose PFA since it preserves the membrane and does not permeabilize the cells (35). No deposition was observed in the presence of fixed cells when treated with different concentrations of Aβ42, indicating that cell function plays an essential role in the deposition of Aβ42 in our model (Fig. 3 *B* and *D*). Notably, staining of both live and fixed sAβ42-treated cells with the Aβ42 antibody 6E10 revealed signals under both conditions, indicating the presence of Aβ in distinct aggregating species: monomers in fixed cells

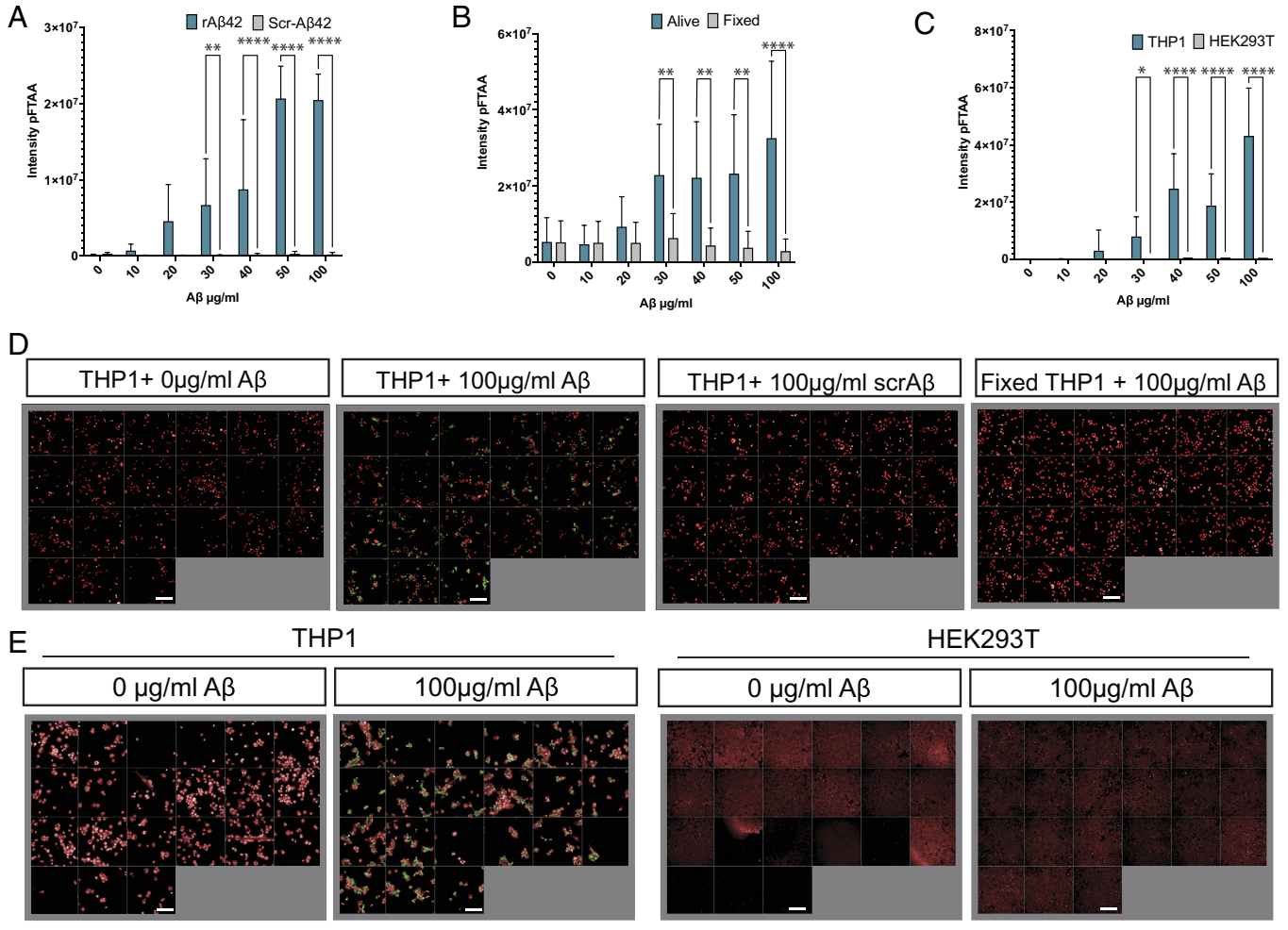

Fig. 3. Aggregation propensity and macrophage viability are needed for Aβ42 deposition. (*A*) pFTAA intensity in cells incubated with rAβ42 or scrambled rAβ42. No aggregation is observed in cells treated with scrambled Aβ42. two independent experiments with four repeats, mean + SD. Statistics: Two-way Anova, with Šídák correction for multiple comparisons. **<0.01, ****<0.0001. (*B*) pFTAA intensity in cells incubated with rAβ42 after or without fixation. Two independent experiments with four repeats, mean + SD. Statistics: Two-way Anova, with Šídák correction for multiple comparisons. **<0.01, ****<0.0001. (*C*) pFTAA intensity of THP-1 macrophages and human embryonic kidney cells (HEK293T) cells treated with increasing concentration of rAβ42. Three independent experiments with four repeats, mean + SD. Statistics: Two-way Anova, with Šídák correction for multiple comparisons. *<0.05, ****<0.0001. (*D*) Representative images of THP-1 cells in different conditions. Each image consists of 21 different fields. Red: nuclei (DAPI), Green: aggregates (pFTAA). (Scale bar, 100 μm.) (*E*) Representative images of THP-1 and HEK cells incubated with or without 100 μg/mL rAβ42. Red: Nuclei (DRAQ7), Green: aggregates (pFTAA). (Scale bar, 100 μm.)

and fibrils in living cells (*SI Appendix*, Fig. S2*E*). Finally, to ensure that macrophage activity is required for Aβ42 deposition, we tested whether another nonmacrophage cell line could cause a similar deposition. We used HEK293T cells for this purpose. When we incubated HEK cells with freshly dissolved Aβ42, we observed some amyloid deposition, but significantly less than that produced by THP-1 cells (Fig. 3 *C* and *E*), consistent with previous results (21). This indicates that macrophages are particularly prone to this amyloid nucleation phenotype, in line with earlier findings (21). To explore whether lysosomal function modulates amyloid deposition, we treated THP-1 macrophages with increasing concentrations of the lysosomal inhibitor chloroquine. Lysosomal inhibition caused a dose-dependent increase in Aβ42 deposition (*SI Appendix*, Fig. S3), consistent with earlier observations that lysosomal dysfunction enhances amyloidogenic processes in microglia (36).

Finally, we wanted to confirm these findings using scanning electron microscopy (SEM). Untreated cells (Fig. 4 *A–C*) appeared morphologically very distinct from treated cells (Fig. 4 *D–F*), again suggesting a cellular response. The space in between cells showed webs of fibrous material in the treated cells (Fig. 4 *F*, *G*, and *K* yellow arrows), that was not found in the sample with untreated cells. Also, amyloid fibrils of Aβ42 grown in a cell-free manner imaged in the same way as the cells, showed a different morphology again (Fig. 4*I*). To ensure that the region with fibril-like assemblies in the treated cells corresponded to the regions of the sample where pFTAA fluorescence was observed, we performed correlative light and electron microscopy (CLEM, Fig. 4 *J–M*). Cells live stained with pFTAA were first imaged using the light microscope; then, after sample preparation, the same cells were imaged using SEM. This confirmed that indeed the extracellular fibril-rich web-like structures correspond to regions of high pFTAA fluorescence and can hence be attributed to Aβ42 fibrils generated by the cells. These correlated fluorescence and ultrastructural data confirm that the extracellular fibrous material visualized by SEM corresponds to the amyloid-positive regions detected in live pFTAA imaging, supporting their identification as Aβ42 fibrils. To further validate the identity of the fibrillar material, THP-1 cells were treated with substoichiometrically HiLyte647-labeled Aβ42. Superresolution fluorescence imaging revealed the same extracellular fibrillar network previously detected by pFTAA and antibody staining (*SI Appendix*, Fig. S4), confirming that these structures represent Aβ42 aggregates produced by the cells.

Therapeutic Antibodies Recognize THP-1 Amyloid Deposition. To determine whether therapeutic antibodies developed to target Aβ fibrils in the human brain could recognize THP-1-generated deposits, we tested four antibodies: Lecanemab, Aducanumab, Donanemab, and Gantenerumab (7, 9–11, 13, 37–39). For specificity, we compared their binding to THP-1-generated Aβ42 aggregates, in vitro-grown Aβ42 fibrils and seeds, as well as the unrelated islet amyloid polypeptide (IAPP) amyloids, which are associated with Type 2 Diabetes.

Using pFTAA staining, we observed that THP-1-generated Aβ42 aggregates displayed higher fluorescence intensity compared to in vitro-grown fibrils and seeds, suggesting distinct properties and potentially different conformations of cell-generated aggregates (Fig. 5*A*). Staining with IAPP and Aβ antibodies confirmed the deposition of each protein and the specificity of the interaction (Fig. 5 *B* and *C*).

Next, we evaluated antibody binding to THP-1-generated Aβ42 and IAPP aggregates, as well as THP-1 cells incubated with in vitro-grown Aβ fibrils and seeds. Both Lecanemab and Aducanemab specifically bound to Aβ42 aggregates but not to IAPP deposits (Fig. 5 *E* and *F*). Donanemab, which targets pyroglutamate-modified Aβ, did not bind to THP-1-generated Aβ42 aggregates, suggesting that these cells may not produce this specific Aβ variant (Fig. 5*G*). Gantenerumab, however, showed nonspecific binding in all conditions, regardless of the presence of Aβ or IAPP (Fig. 5*H*). The concordant staining patterns obtained with multiple Aβ-specific antibodies recognizing distinct epitopes, together with the absence of signal in Aβ-free or scrambled-Aβ42 controls and the lack of cross-reactivity with IAPP amyloids, confirm that the observed deposits represent Aβ42 fibrils rather than nonspecific β-sheet aggregates.

Enhanced Seeding and Cross-Seeding Efficiency of THP-1-Derived Aβ Aggregates. We next evaluated the seeding potential of THP-1cell-derived aggregates. To achieve this, we extracted THP-1 aggregates after 48 h using a standard fibril extraction protocol (40) (Fig. 6*A*). These cell-derived aggregates were then compared to cell-free aggregates and patient-derived aggregates in terms of their seeding efficiency. For this comparison, we utilized an Aβ biosensor cell line (HEK293T cells stably expressing mCherry-Aβ42), which produces high fluorescence intracellular spots upon transfection with potent Aβ42 seeds (41).

The Aβ42 biosensor cells were treated with seeds derived from cell-made fibril extraction, which appeared as fibril fragments by transmission electron microscopy (TEM) (Fig. 6*B*). For comparison, we included amyloids extracted from AD patient brain tissue, and synthetic amyloid fibrils prepared in a cell-free manner, by incubating Aβ42 at 1 mg/mL for 2 wk at room temperature (Fig. 6*C*). Remarkably, the seeding potential of the THP-1-derived fibrils (Fig. 6*D*) was 12-fold higher than that of the cell-free aggregates (Fig. 6 *D* and *E*), but appeared lower than that of patient-derived material.

We also evaluated the cross-seeding potential of THP-1-derived Aβ42 aggregates and cell-free Aβ42 fibrils on HEK293T cells transiently expressing Tau-RD-P301S-eYFP, the so-called tau biosensor line (Fig. 6*A*). Notably, the THP-1-derived Aβ aggregates exhibited a higher cross-seeding efficiency than cell-free fibrils, although this assay showed more variability than the Aβ biosensor (Fig. 6 *F–H*). In this biosensor line, we did not compare to patient brain extracts, since these contain tau seeds, precluding conclusions on cross-seeding.

Overall, these findings highlight the significant influence of the cellular environment on the seeding and cross-seeding potential of Aβ42 aggregates. THP-1-derived amyloids demonstrate significantly greater seeding efficiency than cell-free amyloids, yet they still fall short of the potency exhibited by patient-derived aggregates.

THP-1 and hESC-Derived Microglia Show Similar Early-Stage Responses to Aβ42 Aggregation. We sought to determine whether comparable Aβ deposits could form in the presence of microglia derived from hESCs. To investigate this, we cultured hESC-derived microglia in the presence and absence of Aβ42 for 48 h, followed by staining with pFTAA to detect Aβ42 deposition. Our results confirmed the presence of Aβ42 deposits in these cultures as well (Fig. 7*A*). Given that both THP-1 cells and hESC-derived microglia promote Aβ42 aggregation, we next explored whether these two cell types also exhibit similar cellular responses to Aβ42.

To assess the cellular response of THP-1 cells to Aβ42 treatment, we conducted transcriptomic analysis on differentiated THP-1 cells exposed to varying concentrations of synthetic (s) or recombinant (r) Aβ42 (0 μg/mL, 30 μg/mL, and 100 μg/mL). This analysis revealed over 1,000 differentially expressed genes, including significant upregulation or downregulation of genes associated with cytokine signaling and inflammatory pathways (*SI Appendix*, Figs. S5 and S6).

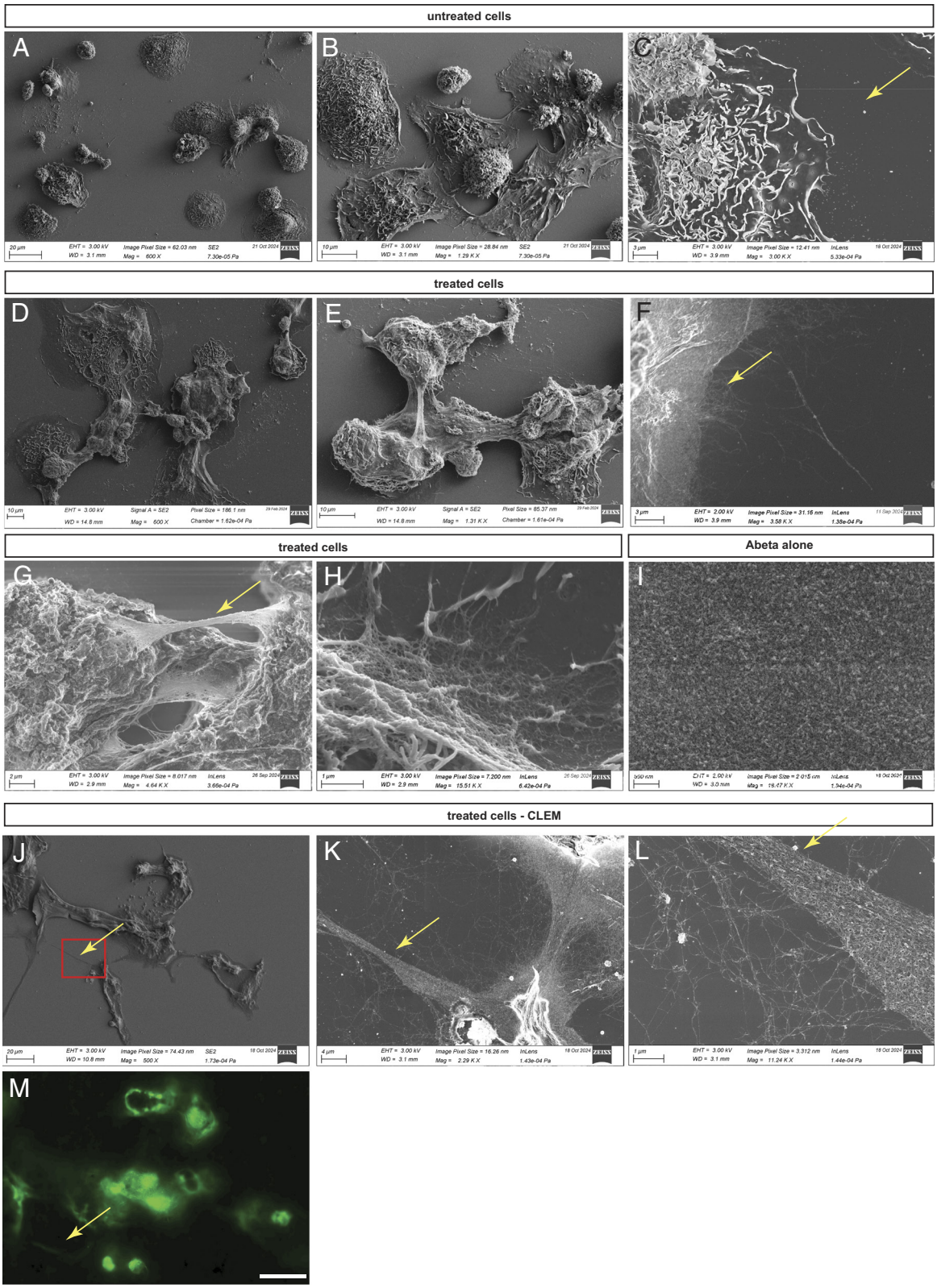

Fig. 4. SEM revealed webs of fibril-like material generated by THP-1 cells in response to Aβ42. (*A–C*) Untreated THP-1 cells. (*D* and *E*) Treated THP-1 cells. (*F–H*) Zoomed-in views of the fibril-like structures formed by THP-1 cells upon sAβ42 treatment. (*I*) Cell-free prepared sAβ42 fibrils imaged in the same manner as the cells. (*J–M*) correlative light and electron microscopy combining fluorescence microscopy and SEM of THP-1 cells exposed to sAβ42 and stained with pFTAA. (Scale bar, for M: 25 μm.)

We compared these differentially expressed genes across the two Aβ42 concentrations with established marker genes representing distinct microglial states, as described in the study by Mancuso et al. (29). In their work, human stem cell–derived microglial precursors were xenografted into *AppNL-G-F* mice and characterized for their response to Aβ states after

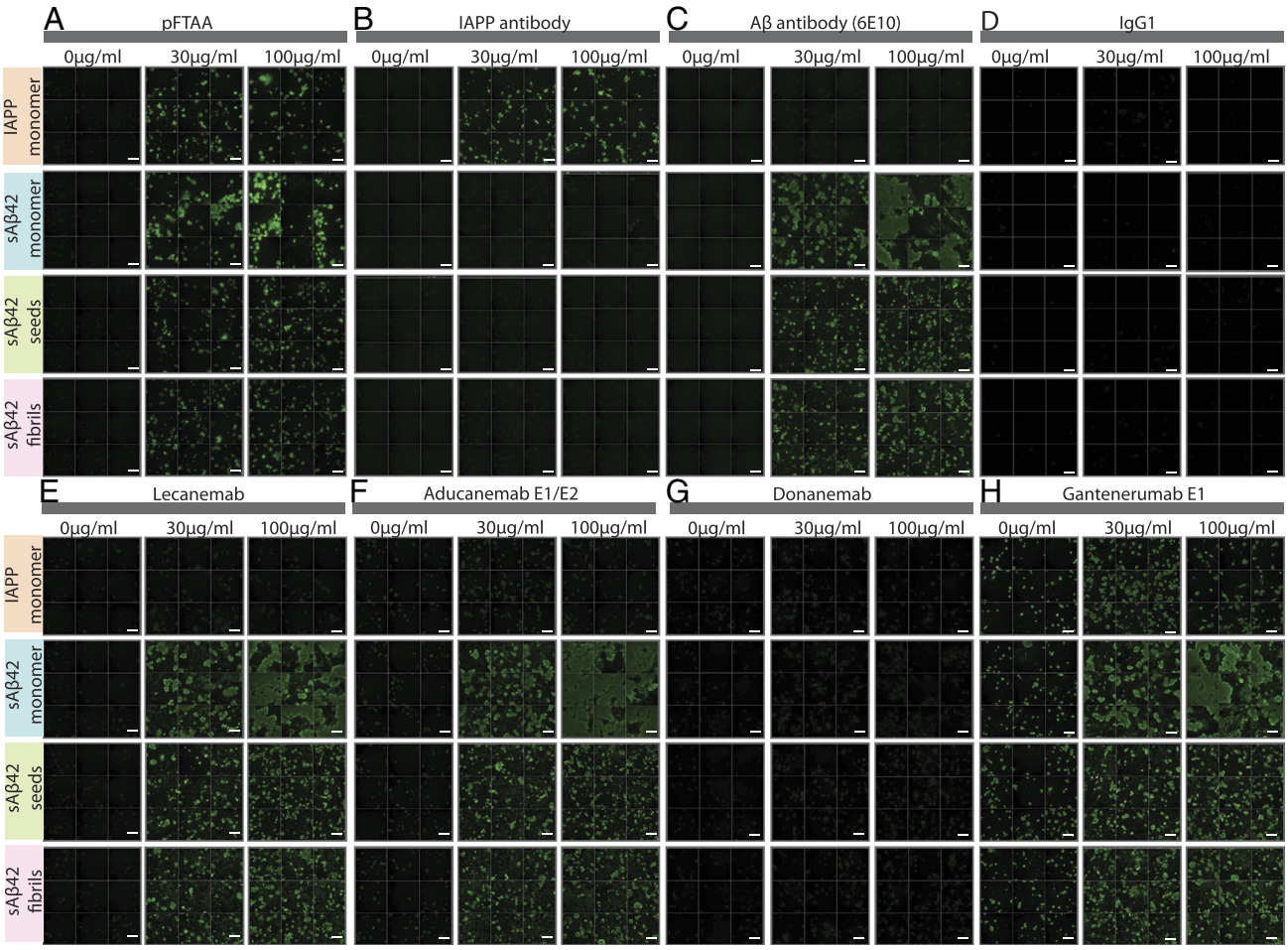

Figure 5

Fig. 5. Recognition of Aβ42 aggregates from THP-1 by therapeutic antibodies. (*A*) pFTAA staining of THP-1 incubated with 0, 30 and 100 μg/mL of IAPP monomer, sAβ42 monomer, sAβ42 cell-free made seeds and fibrils. (Scale bar, 100 μm.) (*B*) IAPP staining of THP-1 incubated with 0, 30 and 100 μg/mL of IAPP monomer, sAβ42 monomer, sAβ42 cell-free made seeds and fibrils. (Scale bar, 100 μm.) (*C*) Aβ staining of THP-1 incubated with 0, 30 and 100 μg/mL of IAPP monomer, sAβ42 monomer, sAβ42 cell-free made seeds and fibrils. (Scale bar, 100 μm.) (*D*) Control staining with IgG1 of THP-1 incubated with 0, 30 and 100 μg/mL of IAPP monomer, sAβ42 monomer, sAβ42 cell-free made seeds and fibrils. (Scale bar, 100 μm.) (*E*) Lecanemab staining of THP-1 incubated with 0, 30 and 100 μg/mL of IAPP monomer, sAβ42 monomer, sAβ42 cell-free made seeds and fibrils. (Scale bar, 100 μm.) (*F*) Aducanemab staining of THP-1 incubated with 0, 30 and 100 μg/mL of IAPP monomer, sAβ42 monomer, sAβ42 cell-free made seeds and fibrils. (Scale bar, 100 μm.) (*G*) Donanemab staining of THP-1 incubated with 0, 30 and 100 μg/mL of IAPP monomer, sAβ42 monomer, sAβ42 cell-free made seeds and fibrils. (Scale bar, 100 μm.) (*H*) Gantenerumab staining of THP-1 incubated with 0, 30 and 100 μg/mL of IAPP monomer, sAβ42 monomer, sAβ42 cell-free made seeds and fibrils. (Scale bar, 100 μm.)

maturation. Our gene set enrichment analysis (GSEA) revealed a downregulation of genes linked to homeostatic microglia and ribosomal function including P2RY12, CX3CR1, and MAF (Fig. 7 *B*, *C*, and *E*). This occurred alongside upregulation of genes involved in cytokine response pathways (CRM-1 and CRM-2) (Fig. 7 *B*–*D*), including upregulation of the proinflammatory cytokines and chemokines IL1B, TNF, and CCL3. Notably, we did not observe major alterations in transcriptional signatures associated with disease-associated microglia (DAM) or HLA, potentially because these responses typically emerge in the presence of amyloid plaques during later disease stages, as noted by Mancuso et al. (29, 42). Nevertheless, the transcriptomic changes we identified align with the characteristic microglial responses to oligomeric Aβ forms, indicating that THP-1 cells effectively replicate early-stage disease responses to Aβ42 pathology.

THP-1 and hESC-Derived Microglia Exhibit Comparable Responses to Genetic Perturbation of TREM2 in Amyloid Deposition. To further validate the THP-1 model as a proxy for microglial responses to amyloid, we assessed the impact of TREM2 perturbation on amyloid deposition using the pFTAA assay. We employed hESC-derived microglia that carry the AD-associated R47H loss-of-function mutation in TREM2 and isogenic wild-type lines used earlier (42, 43), alongside THP-1 cells in which TREM2 was knocked out using CRISPR-Cas9 (Fig. 8*A*). In both models, we observed a marked increase in pFTAA-positive amyloid staining compared to their respective controls, indicating enhanced amyloid deposition (Fig. 8 *B* and *C*). This confirms that impaired TREM2 function facilitates the accumulation of extracellular amyloid fibrils also in our cellular system, consistent with its demonstrated role in enhancing AD risk through limiting beneficial microglial functions, including their recruitment to amyloid plaques. These results support the utility of THP-1 cells as a model for probing microglial responses to amyloid, and further indicate that TREM2 plays a conserved role across phagocytic cells in mediating responses to amyloidogenic peptides. This alignment across cell types supports the use of THP-1 cells as a proxy system to explore microglial biology in the context of AD risk genetics.

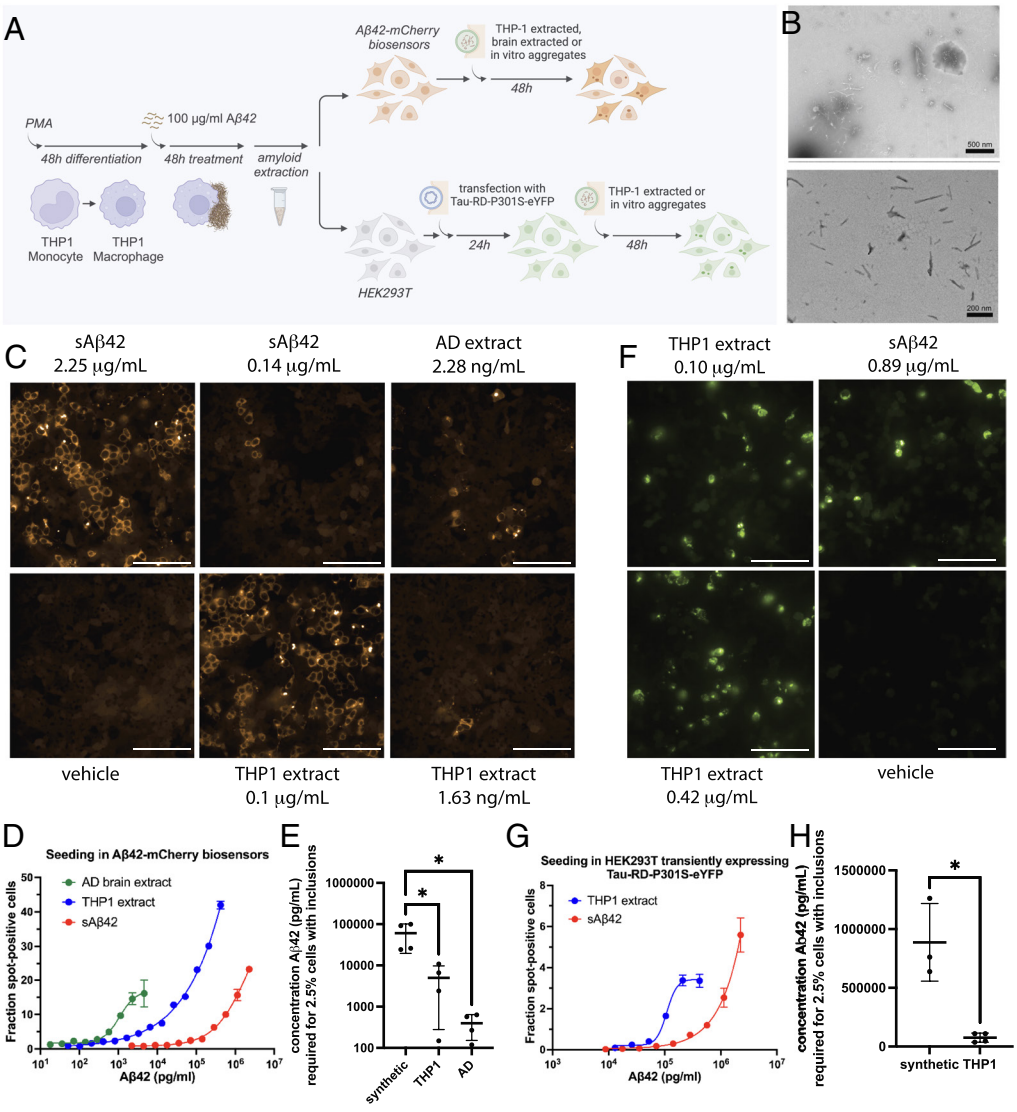

Fig. 6. THP-1-derived aggregates have higher seeding activity than cell-free aggregates. (*A*) Schematic of experimental procedures. (*B*) Transmission electron Microscopy of amyloid fragments of Aβ42 extracted from THP-1 cultures. (*C*) Sample fluorescence microscopy images of Aβ biosensor cells treated with human brain extracts from an AD patient brain, amyloid generated in a cell-free manner, and amyloids extracted from THP-1 cultures, at the doses indicated. (Scale bar, 100 µm.) (*D*) Fraction of spot-positive cells in dose-dependent seeding of Aβ42 biosensor cells with human brain extracts from an AD patient brain, amyloid generated in a cell-free manner, and amyloids extracted from THP-1 cultures. (*E*) Quantification and statistical comparison of the seeding efficiency of different Aβ preparations in Aβ biosensor cells. Seeding efficiency is expressed at the interpolated concentration of Aβ required to obtain 2.5% aggregate positive cells in the high content assay in *D*. Comparisons were performed using one-way ANOVA followed by pairwise comparison using Dunnett's test. *** indicates $P \leq 0.001$. (*F*) Sample fluorescence microscopy images of HEK293T cells expressing Tau-RD-P301S-eYFP treated with amyloid generated in a cell-free manner and amyloids extracted from THP-1 cultures at the doses indicated. (Scale bar, 100 µm.) (*G*) Fraction of spot-positive cells in dose-dependent seeding of Tau biosensor cells with the same samples as in *C*. (*H*) Quantification and statistical comparison of the seeding efficiency in tau biosensor cells, similar to *E*. Statistical comparison was performed using Welch's *t* test.

Discussion

Our study complements recent reports showing that microglia can influence Aβ aggregation dynamics (19). We extend these findings by demonstrating that human macrophage-like cells are capable of remodeling soluble Aβ42 into extracellular fibrillar structures with strong seeding potential. Rather than establishing a primary pathogenic role, these data provide mechanistic support for the concept that phagocytic cells, under specific conditions, can promote the formation of amyloid fibrils alongside their recognized clearance functions. Our work also provides a tractable in vitro model that recapitulates key early microglial responses relevant to AD and enables reproducible generation of seeding-competent amyloid assemblies for mechanistic and therapeutic studies. In particular, we demonstrate that differentiated THP-1 macrophages actively facilitate the extracellular deposition of amyloid fibrils from soluble Aβ42 in a process dependent on cellular activity that remains noncytotoxic within the experimental timeframe. The resulting cell-derived fibrils exhibit unique structural and functional characteristics, distinct from in vitro cell-free Aβ42 fibrils. TEM and amyloid dye binding confirmed these structural differences, while functional assays demonstrated enhanced seeding potency for Aβ42 and cross-seeding efficiency for tau. Whether these differences result from THP-1-induced structural polymorphism, associated cofactors, or both remains an open question. Nonetheless, this model effectively recapitulates early microglial responses to Aβ42, as evidenced by transcriptomic profiling, and highlights its relevance for investigating amyloid propagation and inflammatory mechanisms in AD. This dual validation, at the levels of functional response and genetic susceptibility, positions THP-1 cells as a valuable model system for early AD biology.

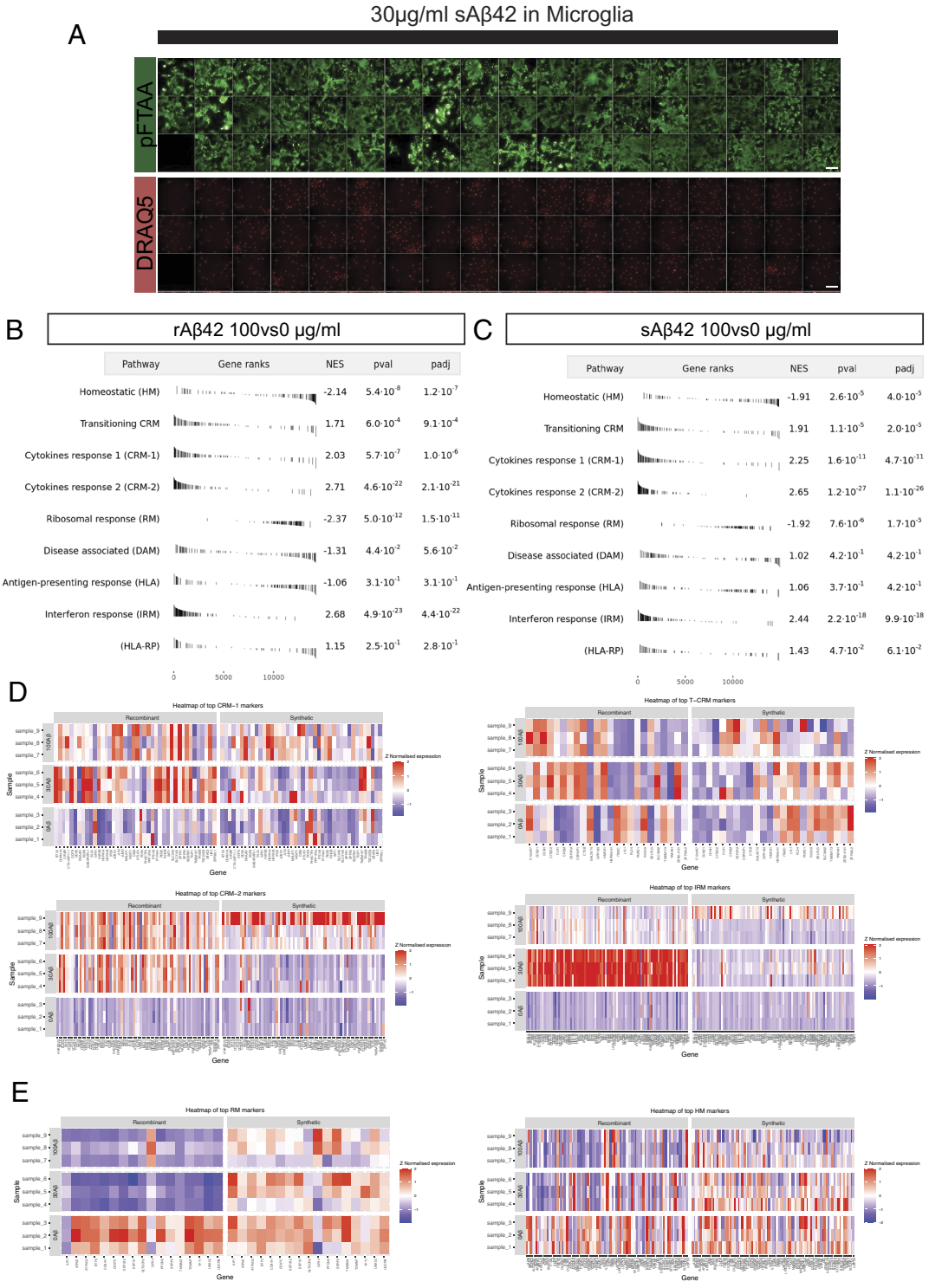

Fig. 7. THP-1 response to Aβ42 is similar to microglia in mouse brains. (*A*) pFTAA and DRAQ5 staining of microglia in the presence of 30 µg/mL indicating Aβ42 deposition. (Scale bar, 100 µm.) (*B*) GSEA of THP-1 cells treated with rAβ42 (recombinant) and compared to previously identified microglia-Aβ pathways. (*C*) GSEA of THP-1 cells treated with sAβ42 (synthetic) and compared to previously identified microglia-Aβ pathways. (*D*) Heatmaps of pathways overrepresented in THP-1 cells in response to rAβ42 or sAβ42. (*E*) Heatmaps of pathways underrepresented in THP-1 cells in response to rAβ42 or sAβ42.

To further contextualize the relevance of the cellular systems used in this study, it is important to consider the evolving understanding of microglial activation states. The traditional M0/M1/M2 nomenclature of microglial activation is no longer supported, as recent single-cell studies reveal a continuum of coexisting transcriptional states even under homeostatic conditions (44–46). The ESC-derived microglia used here have been extensively characterized (42, 47) and acquire a homeostatic-like profile after xenotransplantation, while retaining context-dependent responsiveness to amyloid-β (19). Similarly, THP-1 macrophages mirror iPSC-derived microglia in transcriptional behavior upon amyloid-β exposure (48, 49). These findings confirm that our cellular models are not preactivated but maintain multipotent phenotypes appropriate for mechanistic analyses of microglial responses to Aβ.

Crucially, THP-1 cells not only mirror microglial inflammatory responses but also recapitulate key genetic susceptibility mechanisms.

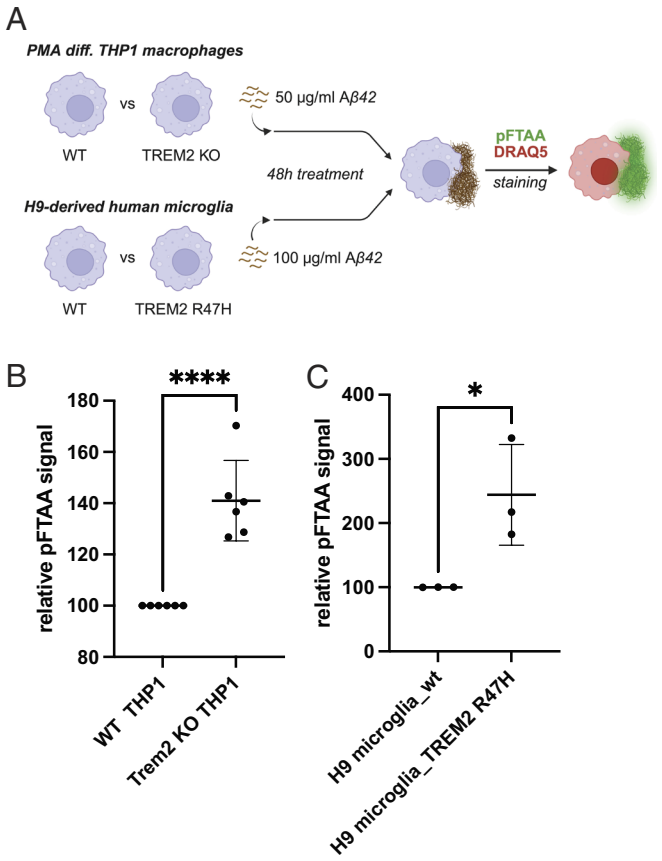

Fig. 8. The effect of TREM2 loss of function on in vitro plaque formation by Aβ42 in THP1 cells is similar to hESC-derived microglia. (*A*) Schematic of experimental procedure. (*B*) pFTAA staining of THP1 cells treated with 50 µg/mL Aβ42. Six independent experiments with five repeats. Statistics: unpaired *t* test. (*C*) pFTAA staining of H9-derived human microglia treated with 100 µg/mL Aβ42. Three independent experiments with seven repeats. Statistics: unpaired *t* test.

Perturbation of TREM2 function, via the Alzheimer-associated R47H variant in hESC-derived microglia or CRISPR-Cas9 knockout in THP-1 cells, resulted in significantly increased Aβ42 deposition. These results support a conserved role for TREM2 across phagocytic cell types in modulating responses to amyloid peptides and highlight the utility of THP-1 cells for mechanistic exploration of AD risk factors. By capturing both the functional and genetic hallmarks of early microglial–amyloid interactions, the THP-1 model offers a uniquely versatile and scalable platform for preclinical exploration.

These findings build upon earlier studies using Aβ40 (21, 22), which is more closely associated with vascular amyloid, but shift the focus to Aβ42, which is more strongly implicated in parenchymal plaque formation and neurotoxicity in AD. While previous research emphasized fibril localization with Aβ40, our study characterizes THP-1-derived Aβ42 aggregates in detail, revealing their potent biological activity. Notably, the fibrils produced by THP-1 cells from Aβ42 demonstrate a 12-fold higher seeding potency compared to cell-free fibrils and an 11-fold increase in tau cross-seeding in biosensor cell lines, underscoring the critical influence of the cellular environment on fibril maturation and the acquisition of disease-relevant structural and functional properties. These distinctions emphasize the importance of investigating different Aβ species (or combinations thereof) in cellular systems to better reflect the heterogeneity of amyloid pathology in vivo.

Amyloid deposition required active phagocytic processes, as demonstrated by the lack of fibril formation in fixed THP1 or nonphagocytic HEK293T cells. The extracellular localization of Aβ42 fibrils, confirmed through fluorescence quenching experiments, highlights macrophages' capacity to promote the accumulation of extracellular aggregates. Our results are in line with the mechanism proposed earlier by Fändrich et al. (21), who suggested that fibril formation is amplified through phagocytic uptake and concentration in endosomal vesicles. However, our data diverge from previous models in showing that extracellular amyloid deposition can occur independently of cell death. This raises a crucial mechanistic question: How do viable phagocytes export amyloid fibrils, and is this process conserved in brain-resident microglia? Future extensions of this system could incorporate mixtures of Aβ isoforms (e.g., Aβ40, Aβ43) to better reflect the heterogeneous composition of plaques in vivo.

In addressing the specificity of amyloid detection, we note that the fibrillar structures identified here were confirmed using multiple orthogonal approaches, including dyes and antibodies recognizing distinct Aβ epitopes. The correlated light and electron microscopy data further demonstrate that the regions of amyloid dye fluorescence correspond precisely to fibrillar ultrastructures, supporting their identification as Aβ42 aggregates.

Transcriptomic analyses reveal that Aβ42 treatment triggers a robust inflammatory response in THP-1 macrophages, characterized by the upregulation of cytokine signaling and immune activation pathways. This profile closely parallels early microglial activation observed in human microglia xenografted into mouse models exposed to amyloid pathology (29), though our in vitro system does not capture the chronic and multicellular context of the diseased brain. The downregulation of homeostatic microglial markers and ribosomal function, alongside the activation of cytokine response pathways, aligns with early-stage responses to oligomeric Aβ (29). However, the absence of DAM or antigen-presenting transcriptional signatures suggests this model is specific to early disease processes, offering a valuable platform for studying initial inflammatory mechanisms and evaluating therapeutic interventions.

In summary, our study identifies macrophage-like cells as active participants in Aβ42 fibril formation in vitro, revealing key differences between cell-derived and synthetic amyloid fibrils in structure, function, and seeding capacity. By reproducing early microglial-like responses to Aβ42, the THP-1 system provides an accessible and genetically tractable platform for modeling amyloid–immune interactions and for generating mechanistic hypotheses about amyloid propagation in AD.

While the THP-1 model offers a tractable and scalable platform to study early amyloid aggregation and inflammatory responses, it has inherent limitations. As a monoculture of peripheral macrophage-like cells, it lacks the full complexity of the central nervous system microenvironment, including interactions with neurons, astrocytes, and vascular elements that shape microglial behavior in vivo. Moreover, the model does not fully recapitulate the chronic stimulation and tissue remodeling present in neurodegenerative disease. This may explain the absence of later-stage transcriptional states such as DAM or antigen-presenting phenotypes, which typically emerge in response to dense plaques and long-term pathology. Despite these constraints, the THP-1 model remains uniquely suited for dissecting acute amyloid–microglia interactions and validating genetic risk factors in a human cellular context. Complementary systems, including human iPSC-derived microglia or in vivo models, remain important for modeling the full spectrum of AD progression.

Future studies using this model could dissect the molecular underpinnings of fibril polymorphism and its impact on amyloid propagation and therapeutic antibody binding. These insights

could inform early-stage therapeutic screening and guide the development of conformation-specific treatments for AD.

Methods Summary. Differentiated THP-1 macrophages and hESC-derived microglia were cultured and treated with Aβ42 under standard conditions. Amyloid formation was assessed using fluorescence and electron microscopy with multiple amyloid-specific dyes and antibodies. Seeding and cross-seeding activity were evaluated with Aβ and tau biosensor cell lines, and transcriptomic responses were analyzed by RNA sequencing. All experimental details, reagent information, and statistical analyses are provided in *SI Appendix*.

Ethics Approval and Consent to Participate. Ethical approval to access and work on the human tissue samples was given by the UZ Leuven ethical committee (Leuven/Belgium; File-No. S63759). An informed consent for autopsy and scientific use of autopsy tissue with clinical information was granted from all subjects involved (case A-21270 with LC ID 93).

Data, Materials, and Software Availability. The RNA sequencing data reported in this paper have been deposited in the Gene Expression Omnibus (GEO) database under accession number GSE319445 (50). Other data are included in the article and/or *SI Appendix*.

ACKNOWLEDGMENTS. We gratefully acknowledge the Bio Imaging Core, Department of Neurosciences KU Leuven, VIB–KU Leuven Center for Brain & Disease Research for their support and assistance in this work. Light and electron microscopy imaging was performed at the VIB Bioimaging Core Leuven. In particular, we thank Nikky Corthout of the VIB Bio Imaging Core Leuven for her support and assistance with light microscopy imaging. Library preparation, sequencing, and statistical data analysis were performed by VIB Nucleomics Core (https://nucleomicscore.sites.vib.be/en). This work was supported by the Flanders institute for Biotechnology (VIB); KU Leuven (Postdoctoral Fellowship PDMT2/22/059 to K.K.); the Fund for Scientific Research Flanders (FWO, project grant G0C3522N to F.R., and Postdoctoral Fellowship 1223924 N to K.K. and 12AWB24N to B.P.); the Stichting Alzheimer Onderzoek (SAO-FRA 2020/0030 and 2025/0037); and the National Institutes of Ageing of the NIH, USA, under award number US R01AG079234. Neuropathological characterization of human brain samples was supported by FWO grants (G0F8516N and G065721N) to D.R.T. The content is solely the responsibility of the authors and does not necessarily represent the official views of the NIH.

Author affiliations: [a]Switch Laboratory, VIB-KU Leuven Center for Neuroscience, VIB, Leuven 3000, Belgium; [b]Switch Laboratory, Department of Cellular and Molecular Medicine, University of Leuven (KU Leuven), Leuven 3000, Belgium; [c]Department of Neurosciences, University of Leuven (KU Leuven), Leuven 3000, Belgium; [d]Bio Imaging Core, VIB, Leuven 3000, Belgium; [e]Laboratory for Therapeutic and Diagnostic Antibodies, Department of Pharmaceutical and Pharmacological Sciences, University of Leuven (KU Leuven), Leuven, Flemish Brabant 3000, Belgium; [f]PharmAbs, University of Leuven (KU Leuven) Antibody Center, KU Leuven, Leuven, Flemish Brabant 3000, Belgium; [g]University of Leuven (KU Leuven), Leuven Brain Institute, Leuven 3000, Belgium; [h]Laboratory for Neuropathology, University of Leuven (KU Leuven), and Department of Pathology, University Hospitals Leuven, Leuven 3000, Belgium; [i]Biomedical Center, Biochemistry, Faculty of Medicine, Ludwig-Maximilians-Universität München, Munich 82152, Germany; [j]Neuroimmunology and Neurodegenerative Diseases, German Center for Neurodegenerative Diseases, Munich 81377, Germany; and [k]Munich Cluster for Systems Neurology, Munich 82152, Germany

1. Alzheimer's Association, 2019 Alzheimer's disease facts and figures includes a special report on Alzheimer's detection in the primary care setting: Connecting patients and physicians (2019).
2. Alzheimer's Disease International, O. World Alzheimer report 2015 the global impact of dementia (2015).
3. J. A. Hardy, G. A. Higgins, Alzheimer's disease: The amyloid cascade hypothesis. *Science* **256**, 184–185 (1992).
4. D. Scheuner *et al.*, Secreted amyloid beta-protein similar to that in the senile plaques of Alzheimer's disease is increased in vivo by the presenilin 1 and 2 and APP mutations linked to familial Alzheimer's disease. *Nat. Med.* **2**, 864–870 (1996).
5. N. Suzuki *et al.*, An increased percentage of long amyloid beta protein secreted by familial amyloid beta protein precursor (beta APP717) mutants. *Science* **264**, 1336–1340 (1994).
6. Z. He *et al.*, Amyloid-beta plaques enhance Alzheimer's brain tau-seeded pathologies by facilitating neuritic plaque tau aggregation. *Nat. Med.* **24**, 29–38 (2018), 10.1038/nm.4443.
7. L. Soderberg *et al.*, Lecanemab, aducanumab, and gantenerumab–Binding profiles to different forms of amyloid-beta might explain efficacy and side effects in clinical trials for Alzheimer's disease. *Neurotherapeutics* **20**, 195–206 (2023), 10.1007/s13311-022-01308-6.
8. P. Yang, F. Sun, Aducanumab: The first targeted Alzheimer's therapy. *Drug Discov. Ther.* **15**, 166–168 (2021), 10.5582/ddt.2021.01061.
9. A. J. Espay, K. P. Kepp, K. Herrup, Lecanemab and donanemab as therapies for Alzheimer's disease: An illustrated perspective on the data. *eNeuro* **11**, ENEURO.0319-23.2024 (2024), 10.1523/ENEURO.0319-23.2024.
10. V. Volloch, S. Rits-Volloch, Effect of lecanemab and donanemab in early Alzheimer's disease: Mechanistic interpretation in the amyloid cascade hypothesis 2.0 perspective. *J. Alzheimers Dis.* **93**, 1277–1284 (2023), 10.3233/Jad-230164.
11. T. A. Bayer, Pyroglutamate Abeta cascade as drug target in Alzheimer's disease. *Mol. Psychiatry* **27**, 1880–1885 (2022), 10.1038/s41380-021-01409-2.
12. B. H. Kim *et al.*, Second-generation anti-amyloid monoclonal antibodies for Alzheimer's disease: Current landscape and future perspectives. *Transl. Neurodegener.* **14**, 6 (2025), 10.1186/s40035-025-00465-w.
13. M. A. Mintun *et al.*, Donanemab in early Alzheimer's disease. *N. Engl. J. Med.* **384**, 1691–1704 (2021), 10.1056/NEJMoa2100708.
14. J. Frackowiak *et al.*, Ultrastructure of the microglia that phagocytose amyloid and the microglia that produce beta-amyloid fibrils. *Acta Neuropathol.* **84**, 225–233 (1992), 10.1007/BF00227813.
15. D. V. Hansen, J. E. Hanson, M. Sheng, Microglia in Alzheimer's disease. *J. Cell Biol.* **217**, 459–472 (2018), 10.1083/jcb.201709069.
16. P. d'Errico *et al.*, Microglia contribute to the propagation of Abeta into unaffected brain tissue. *Nat. Neurosci.* **25**, 20–25 (2022), 10.1038/s41593-021-00951-0.
17. S. H. Baik, S. Kang, S. M. Son, I. Mook-Jung, Microglia contributes to plaque growth by cell death due to uptake of amyloid beta in the brain of Alzheimer's disease mouse model. *Glia* **64**, 2274–2290 (2016), 10.1002/glia.23074.
18. E. Spangenberg *et al.*, Sustained microglial depletion with CSF1R inhibitor impairs parenchymal plaque development in an Alzheimer's disease model. *Nat. Commun.* **10**, 3758 (2019), 10.1038/s41467-019-11674-z.
19. N. Baligacs *et al.*, Homeostatic microglia initially seed and activated microglia later reshape amyloid plaques in Alzheimer's disease. *Nat. Commun.* **15**, 10634 (2024), 10.1038/s41467-024-54779-w.
20. Y. Chen, M. Colonna, Two-faced behavior of microglia in Alzheimer's disease. *Nat. Neurosci.* **25**, 3–4 (2022), 10.1038/s41593-021-00963-w.
21. R. P. Friedrich *et al.*, Mechanism of amyloid plaque formation suggests an intracellular basis of Abeta pathogenicity. *Proc. Natl. Acad. Sci. U.S.A.* **107**, 1942–1947 (2010), 10.1073/pnas.0904532106.
22. S. Han *et al.*, Amyloid plaque structure and cell surface interactions of beta-amyloid fibrils revealed by electron tomography. *Sci. Rep.* **7**, 43577 (2017), 10.1038/srep43577.
23. T. Masuda, Common and distinct features of diverse macrophage populations in the central nervous system. *Proc. Jpn. Acad. Ser. B Phys. Biol. Sci.* **101**, 216–223 (2025), 10.2183/pjab.101.013.
24. J. D. Ulrich, D. M. Holtzman, TREM2 function in Alzheimer's disease and neurodegeneration. *ACS Chem. Neurosci.* **7**, 420–427 (2016), 10.1021/acschemneuro.5b00313.
25. R. Sims *et al.*, Rare coding variants in PLCG2, ABI3, and TREM2 implicate microglial-mediated innate immunity in Alzheimer's disease. *Nat. Genet.* **49**, 1373–1384 (2017), 10.1038/ng.3916.
26. R. Guerreiro *et al.*, TREM2 variants in Alzheimer's disease. *N. Engl. J. Med.* **368**, 117–127 (2013), 10.1056/NEJMoa1211851.
27. T. R. Jay *et al.*, TREM2 deficiency eliminates TREM2+ inflammatory macrophages and ameliorates pathology in Alzheimer's disease mouse models. *J. Exp. Med.* **212**, 287–295 (2015), 10.1084/jem.20142322.
28. Y. Wang *et al.*, TREM2 lipid sensing sustains the microglial response in an Alzheimer's disease model. *Cell* **160**, 1061–1071 (2015), 10.1016/j.cell.2015.01.049.
29. R. Mancuso *et al.*, Xenografted human microglia display diverse transcriptomic states in response to Alzheimer's disease-related amyloid-beta pathology. *Nat. Neurosci.* **27**, 886–900 (2024), 10.1038/s41593-024-01600-y.
30. J. I. R. Dijkstra *et al.*, TREM2 risk variants and associated endophenotypes in Alzheimer's disease. *Alzheimers Res. Ther.* **17**, 57 (2025), 10.1186/s13195-025-01700-2.
31. E. I. Yakupova, L. G. Bobyleva, I. M. Vikhlyantsev, A. G. Bobylev, Congo red and amyloids: History and relationship. *Biosci. Rep.* **39**, BSR20181415 (2019), 10.1042/bsr20181415.
32. J. Brelstaff *et al.*, The fluorescent pentameric oligothiophene pFTAA identifies filamentous tau in live neurons cultured from adult P301S tau mice. *Front. Neurosci.* **9**, 184 (2015), 10.3389/fnins.2015.00184.
33. A.-M. Fernandez-Escamilla, F. Rousseau, J. Schymkowitz, L. Serrano, Prediction of sequence-dependent and mutational effects on the aggregation of peptides and proteins. *Nat. Biotechnol.* **22**, 1302–1302 (2004).
34. J. A. J. Housmans, G. Wu, J. Schymkowitz, F. Rousseau, A guide to studying protein aggregation. *FEBS J.* **290**, 583 (2021), 10.1111/febs.16312.
35. A. J. Hobro, N. I. Smith, An evaluation of fixation methods: Spatial and compositional cellular changes observed by Raman imaging. *Vib. Spectrosc.* **91**, 31–45 (2017), 10.1016/j.vibspec.2016.10.012.
36. S. Kaji *et al.*, Apolipoprotein E aggregation in microglia initiates Alzheimer's disease pathology by seeding beta-amyloidosis. *Immunity* **57**, 2651–2668.e2612 (2024), 10.1016/j.immuni.2024.09.014.
37. K. I. Avgerinos, L. Ferrucci, D. Kapogiannis, Effects of monoclonal antibodies against amyloid-β on clinical and biomarker outcomes and adverse event risks: A systematic review and meta-analysis of phase III RCTs in Alzheimer's disease. *Ageing Res. Rev.* **68**, 101339 (2021), 10.1016/j.arr.2021.101339.
38. R. J. Bateman *et al.*, Gantenerumab: An anti-amyloid monoclonal antibody with potential disease-modifying effects in early Alzheimer's disease. *Alzheimers Res. Ther.* **14**, 178 (2022), 10.1186/s13195-022-01110-8.
39. R. J. Bateman *et al.*, Two phase 3 trials of gantenerumab in early Alzheimer's disease. *N. Engl. J. Med.* **389**, 1862–1876 (2023), 10.1056/NEJMoa2304430.
40. K. Annamalai *et al.*, Polymorphism of amyloid fibrils in vivo. *Angew. Chem. Int. Ed. Engl.* **55**, 4822–4825 (2016), 10.1002/anie.201511524.
41. K. Konstantoulea *et al.*, Heterotypic Amyloid beta interactions facilitate amyloid assembly and modify amyloid structure. *EMBO J.* **41**, e108591 (2022), 10.15252/embj.2021108591.

42. R. Mancuso *et al.*, Stem-cell-derived human microglia transplanted in mouse brain to study human disease. *Nat. Neurosci.* **22**, 2111–2116 (2019), 10.1038/s41593-019-0525-x.
43. C. Claes *et al.*, Human stem cell–derived monocytes and microglia-like cells reveal impaired amyloid plaque clearance upon heterozygous or homozygous loss of TREM2. *Alzheimers Dement.* **15**, 453–464 (2019), 10.1016/j.jalz.2018.09.006.
44. R. C. Paolicelli *et al.*, Microglia states and nomenclature: A field at its crossroads. *Neuron* **110**, 3458–3483 (2022), 10.1016/j.neuron.2022.10.020.
45. H. Keren-Shaul *et al.*, A unique microglia type associated with restricting development of Alzheimer's disease. *Cell* **169**, 1276–1290.e1217 (2017), 10.1016/j.cell.2017.05.018.
46. T. R. Hammond *et al.*, Single-cell RNA sequencing of microglia throughout the mouse lifespan and in the injured brain reveals complex cell-state changes. *Immunity* **50**, 253–271.e256 (2019), 10.1016/j.immuni.2018.11.004.
47. A. F. Lloyd *et al.*, Deep proteomic analysis of microglia reveals fundamental biological differences between model systems. *Cell Rep.* **43**, 114908 (2024), 10.1016/j.celrep.2024.114908.
48. M. J. Dolan *et al.*, Exposure of iPSC-derived human microglia to brain substrates enables the generation and manipulation of diverse transcriptional states in vitro. *Nat. Immunol.* **24**, 1382–1390 (2023), 10.1038/s41590-023-01558-2.
49. A. Podlesny-Drabiniok *et al.*, BHLHE40/41 regulate microglia and peripheral macrophage responses associated with Alzheimer's disease and other disorders of lipid-rich tissues. *Nat. Commun.* **15**, 2058 (2024), 10.1038/s41467-024-46315-7.
50. K. Konstantoulea *et al.*, Phagocytes as plaque catalysts: Human macrophages generate seeding-competent Aβ42 fibrils with cross-seeding activity. Gene Expression Omnibus. https://www.ncbi.nlm.nih.gov/geo/query/acc.cgi?acc=GSE319445. Deposited 12 February 2026.